Shock Waves (1994) 3:167–179

Shock Waves

Shock wave interaction with cellular materials

Part II: open cell foams; experimental and numerical results

G. Ben-Dor[1], G. Mazor[1], O. Igra[1], S. Sorek[1], and H. Onodera[2]

[1] Pearlstone Center for Aeronautical Engineering Studies, Department of Mechanical Engineering, Ben-Gurion University of the Negev, Beer Sheva, Israel
[2] Department of Mechanical Engineering, Iwate University, Morioka, Japan

Received May 5, 1992; accepted July 11, 1992

Abstract. In the Part I of this study, namely the analytical part in Mazor et al. (1992), the governing equations of the phenomenon in which a planar shock wave collides head-on with a cellular material and interacts with it were developed using a Lagrangian approach. In addition, the numerical approach adopted by us during the numerical course of this study was briefly outlined there. The present part reports on experimental and numerical results of the head-on reflection of a planar shock wave with an open cell polyurethane foam. Foams as mentioned by Gibson and Ashby (1988) and summerized in Part I of this study by Mazor et al. (1992), are one of the two general types of cellular materials.

Key words: Cellular material, Experiment, Shock wave propagation, Two-phase flow

1. Introduction

The problem under consideration is shown schematically in Fig. 1. The cellular material in the present study is a foam which, as definded by Gibson and Ashby (1988), has in general polyhedra cells which pack in three-dimensions to fill a space. In addition, foams can be devided into: open cell foams in which the cells connect through open faces; and closed cell foams in which each cell is sealed off from its neighboring cells.

The schematic illustration of the problem under investigation, shown in Fig. 1, indicates that owing to the side-walls of the shock tube the foam cannot expand in the y- and z-directions. Hence the foam, which can be compressed only in the x-direction, experiences during the head-on collision with the planar shock wave a uni-axial strain compression, i.e., $\varepsilon_x \neq 0$, $\varepsilon_y = 0$, and $\varepsilon_z = 0$, where ε_i is the strain in the i-th direction. As a result of this compression mode, stresses are developed in the foam both in the x-, y- and z-directions, i.e., $\sigma_x \neq 0$, $\sigma_y \neq 0$, and $\sigma_z \neq 0$.

Correspondence to: G. Ben-Dor

The analytical investigation in Part I of this study, Mazor et al. (1992) resulted in a set of ten governing equations, namely,
– the conservation of mass of the gaseous phase,
– the definition of the gas particles velocity,
– the conservation of linear momentum of the gaseous phase,
– the conservation of energy of the gaseous phase,
– the equation of state of the gaseous phase,
– the conservation of mass of the cellular material,
– the definition of the cellular material particles velocity,
– the equation of motion of the cellular material,
– the definition of the strain in the x-direction (in the cellular material), and
– the stress-strain relation of the cellular material.

As mentioned in Part I of this study, out of the foregoing listed ten governing equations the last one, namely the stress-strain relation of the cellular material, is most significant as it dictates how a cellular material, in general, and a foam, in particular, will respond to the sudden loading imposed on it by a head-on collision of shock waves.

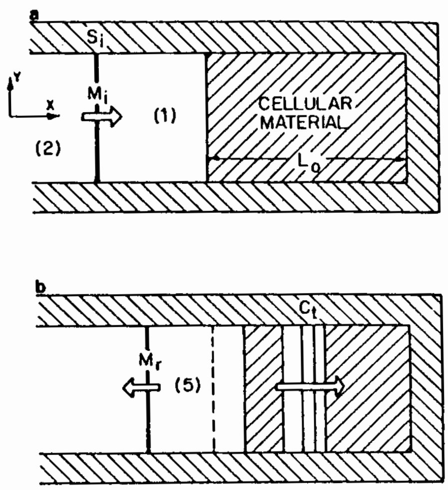

Fig. 1a,b. Schematic illustration of the investigated interaction

Based on the stress-strain relation of foams they can be devided into three types, for details see Gibson and Ashby (1988): elastomeric foams; elastic-plastic foams; and elastic-brittle foams.

Schematic illustrations of the general shapes of the stress-strain relations of these three types of foams are shown in Fig. 2. They all show linear elasticity at low stresses, followed by a long collapse plateau, truncated by a regime of densification in which the stress rises steeply. The main differece between the three types of the foams is in the mechanical behavior in their plateau regime. In elastomeric foams the plateau is due to elastic buckling of the cell walls, in elastic-plastic foams the plateau arises from plastic yielding of the cell walls and in elastic-brittle foams the plateau is due to brittle crushing of the cell walls.

As a consequence of the foregoing description it is clear that in general there are six different combinations of foam types which arise from the fact that there are three different mechanical behaviors in the plateau regime (elastomeric, elastic-plastic and elastic-brittle) and two different types of cellular structures (open and closed cells).

In order to demonstrate the effect of the structure on the mechanical behavior of the foam, let us consider only the linear elastic domain of the stress-strain curve. For the three types of the foams shown in Fig. 2 the stress-strain relation in the linear elastic domain is,

$$\sigma = E_c \varepsilon$$

where

$$E_c = \begin{cases} E_s \left(\dfrac{\rho_c}{\rho_s}\right)^2, & \text{open-cell}, \quad (1) \\[2ex] E_s \varphi^2 \left(\dfrac{\rho_c}{\rho_s}\right)^2 + (1-\varphi)\dfrac{\rho_c}{\rho_s} \\ \quad + \dfrac{P_0}{E_s} \dfrac{1-2\nu_c}{1-\dfrac{\rho_c}{\rho_s}}, & \text{closed-cell} \quad (2) \end{cases}$$

where ν_c is the Poisson ratio of the foam (usually taken as 1/3 in the linear elastic regime), P_0 is the initial pressure inside the pores, φ is a constant (usually having a value $0.6 \div 0.8$), and E is the Young modulus. Subscripts c and s denote, respectively, the cellular material (foam in the present case) and the solid material from which the foam is made (polyurethane in the present case). The role of the relative density, ρ_c/ρ_s, which was referred to in Part I of this study, as the most important property of a cellular material is clearly evident in (2). It is also evident from (2) that while the initial pressure, P_0, plays a significant role in the mechanical behavior of closed cell foams, it has practically, as expected, no effect on the mechanical behavior of open cell foams.

The interest in better understanding the head-on reflection of a planar shock wave from a foam has grown quite intensively in the past decade. However, most of the reported researches related to this problem were experimental. Figure 3 is a reproduction of some of the experimental results of Gvozdeva et al. (1985) which were conducted using a polyurethane foam ($\rho_c = 33\,\mathrm{kg/m^3}$ and $\phi = 0.95 \div 0.98$, where ϕ is the porosity). As can be seen from this figure:

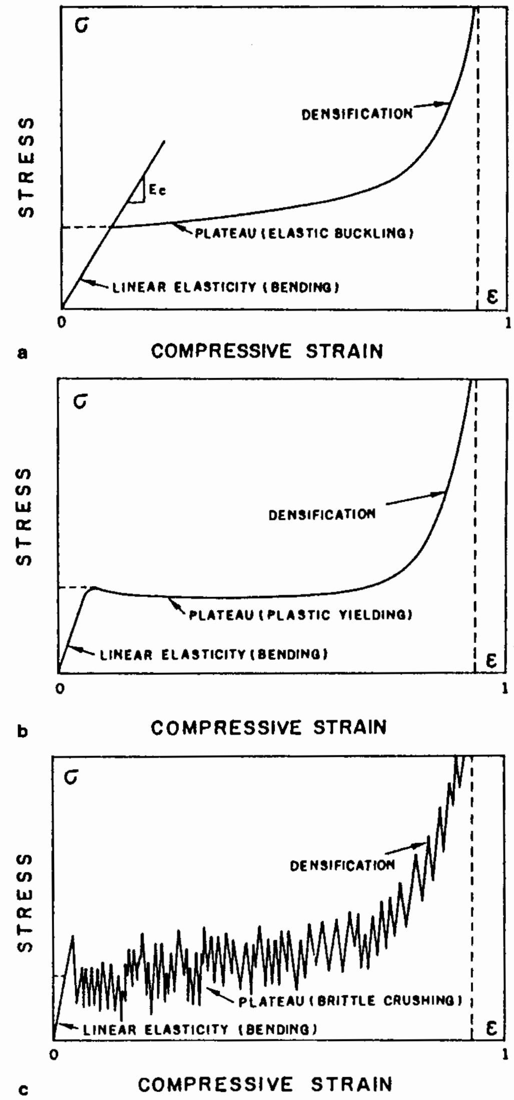

Fig. 2a–c. General shape of the stress-strain relation curves for: **a** elastomeric foam; **b** elastic-plastic foam; **c** elastic-brittle foam

(1) The peak pressure acting on the shock-tube end-wall, $P_{w,max}$, behind the foam is higher than the the pressure, P_5, which would have been obtained had the incident shock wave reflected head-on from the end-wall of the shock tube without the presence of a foam;

(2) The peak pressure, $P_{w,max}$, increases as the initial length of the foam increases;

(3) In spite of the above remark it is also evident from Fig. 3 that as the initial length of the foam increases the increase in the peak pressure seems to approach an asymptotic value. Hence, increasing the initial length of the foam beyond a certain value will not affect the peak pressure anymore.

Note that while the pressure enhancement at the shock-tube end-wall which was mentioned in the above first remark agrees with the analytical considerations which were presented in Part I of this study, Mazor et al. (1992), the experimental observations mentioned in the second and the third remarks are to be explained.

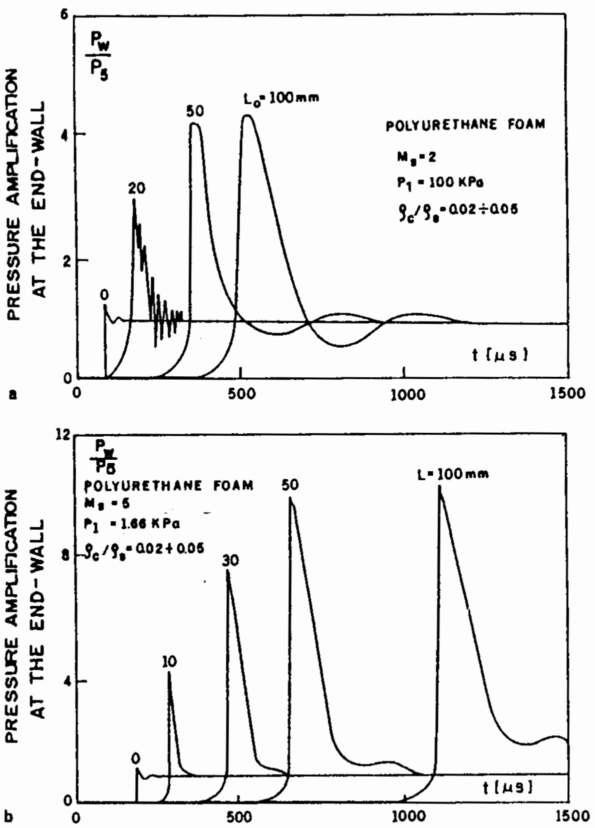

Fig. 3a,b. The pressure histories at the shock tube end-wall as recorded by Gvozdeva et al. (1985) for a polyurethane foam and: **a** $M_s = 2$; **b** $M_s = 5$

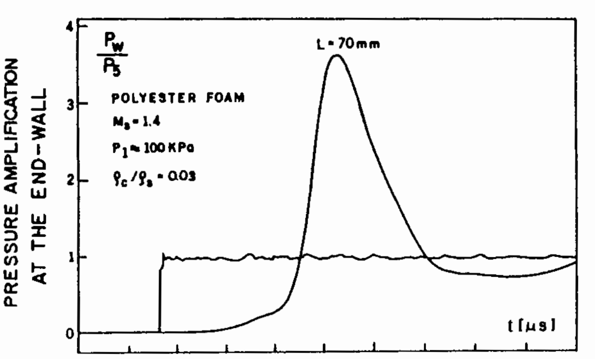

Fig. 4. The pressure history at the shock-tube end-wall as recorded by Skews et al. (1992) for a polyurethane foam and $M_s = 1.4$

Similar pressure measurments indicating the pressure amplification as a result of reflecting the incident shock wave head-on from a foam rather than the shock-tube end-wall were presented recently by Skews et al. (1992). Figure 4 is a reproduction of their pressure measurements in the case of a polyester foam ($\rho_c = 38\,\mathrm{kg/m^3}$ and $\phi = 0.97$). Beside the fact that the pressure profile shown in Fig. 4 is similar to those shown in Fig. 3, it should be noted that it seems that the impulse generated by the two pressure profiles, i.e., with and without the presence of a foam are almost identical.

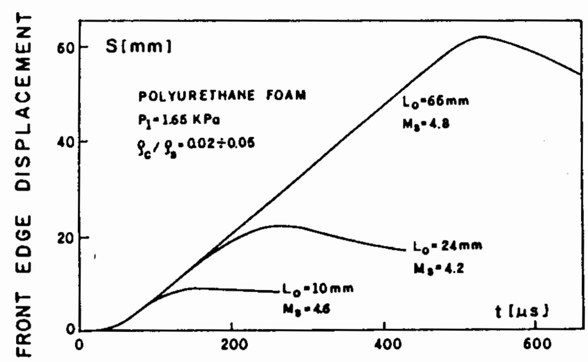

Fig. 5. The displacement of the front face of the foam as recorded by Gvozdeva et al. (1985)

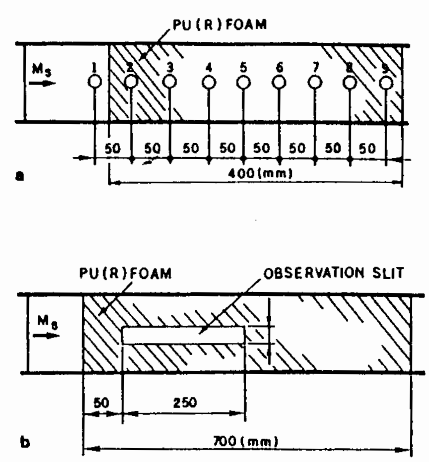

Fig. 6. The experimental set-ups used in the present study **a** for pressure and front face displacement measurements and **b** for holographic interferometry mesurements of the waves propagating inside the foam

The displacement of the front face of the foam as obtained experimentally by Gvozdeva et al. (1985) is shown in Fig. 5. It is evident from this figure that beside the very early stage of the compression, the front face of the foam moves at a constant velocity. Similar to the above remark this behavior of the foam has also not been explained yet.

The above mentioned results regarding the behavior of a foam collided head-on with a planar shock wave, being not intuitive and partially yet unexplained, motivated us to undertake the present study. The main purposes of this study were:

(1) to investigate experimentally the problem under consideration in order to better understand the phenomenon and the parameters affecting it; and
(2) to develop a simulation code capable of reproducing the above presented results.

It should be mentioned here that during the review process of the present paper a numerical simulation of experiments by Skews (1991) was published by Baer (1992). Predictions of his numerical code were in very good agreement with the Skews' experimental results.

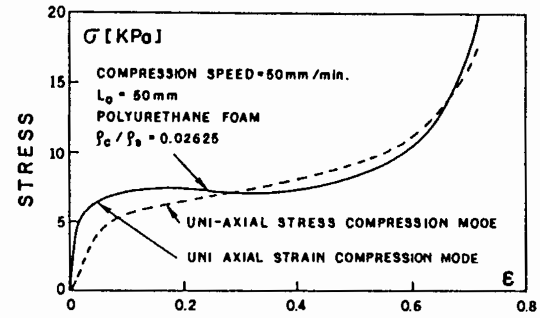

Fig. 7. The stress-strain curve of the investigated foam

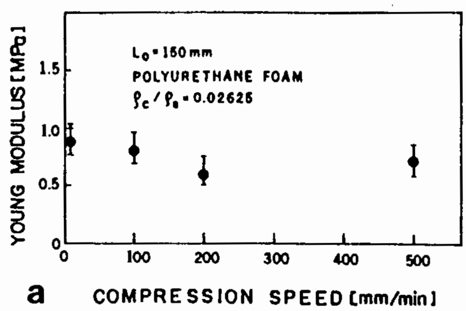

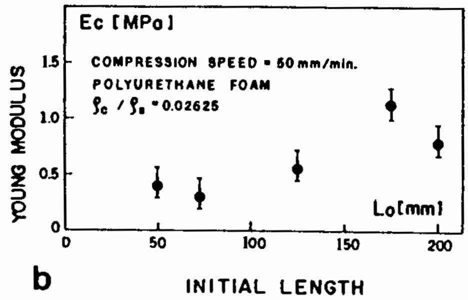

Fig. 8a,b. The dependence of the Young modulus on: **a** the compression speed; **b** the initial length of the foam

2. Present study

As mentioned in the foregoing introduction the present study consisted of an experimental part and a numerical one. As a consequence, in the following, these two parts will be described separately. It should also be noted that due to the difficulty in measuring some of the mechanical properties of foams, which are essential to carrying out a numerical simulations, most of the following comparisons between the experimental results and the numerical predictions will be only qualitative. In order to overcome this shortcoming there is a need to develop experimental techniques capable of acurately measuring the required mechanical properties of foams.

2.1. The experimental study

Open cell flexible polyurethane foam PU(R) was used in the present experiments. Based on manufacturer's data the density of the foam was $\rho_c = 31.5\,\text{kg/m}^3$ while the density of the pure rigid polyurethane, as given by Gibson and Ashby (1988), is about $1200\,\text{kg/m}^3$. This values result in a relative density of about $\rho_c/\rho_s = 0.02625$ which in turn results in a porosity of about $\phi = 0.97375$, see in (8).

The experiments were conducted in a 60 mm × 150 mm shock tube of the Shock Wave Research Center of the Institute of Fluid Science, Tohoku University. The major experimental set-up is shown in Fig. 6a. The foam was a solid piece and 400 mm long. Nine pressure transducers (Kistler model 603B) were flush mounted, 50 mm apart, on the shock-tube side-walls. The first pressure transducer was located 25 mm ahead of the front face of foam and hence it recorded the pressure changes across both the incident shock wave and the reflected shock wave from the front face of the foam (S_i and S_r respectively, in Fig. 1).

The experimental set-up shown in Fig. 6b was used for flow visualization (holographic interferometry) of the waves propagating inside the foam. For this case a 20 mm×250 mm slit was cut in the foam along its centerline. The leading opening of the slit was located 50 mm away from the front face of the foam. The total length of the foam in this series of experiments was 700 mm.

The stress-strain relation of the foam was measured using a SHIMAZUmaterial testing machine (Auto-Graph AG 5000-C). This machine enables one to control the compression speed. A typical stress-strain curve as obtained for a 50 mm long foam and a compression speed of 50 mm/min is shown in Fig. 7. The dashed line was obtained in a uni-axial stress compression and the solid line in a uni-axial strain compression, which, as mentioned earlier, was the actual compression mode during the present experimental study.

Figure 7 indicates that in addition to the dependence of the stress-strain relation of a foam on its mechanical behavior in the plateau regime (see Fig. 2) as well as on the internal structure of the foam (open or closed cells) it also depends on the compression mode, i.e., uni-axial strain, uni-axial stress and perhaps bi-axial stress too, which has not been investigated throughout the course of this study. Furthermore, the present experimental study revealed that in addition to the above mentioned parameters the stress-strain relation of the investigated foam depends on its initial length and on the compression rate, which, as mentioned earlier, could be controled, to some extent, by the material testing machine.

By measuring the slope of the stress-strain curve in its elastic regime the Young modulus of the investigated foam could be deduced. The dependence of the Young modulus of the investigated foam on the compression speed for a constant initial length and on its initial length for a fixed compression speed are shown in Fig. 8a and 8b, respectively. While the Young modulus seems slightly to decrease when the compression speed is increased, it exhibits, in general, a noticable increase when its initial length is increased, e.g., from about 0.4 MPa when its length is 50 mm to about 1.1 MPa when its length is increased to 175 mm.

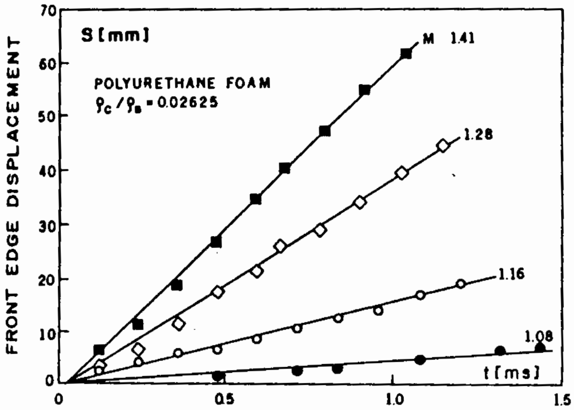

Fig. 9. The displacement of the front face of the foam for different incident shock Mach numbers

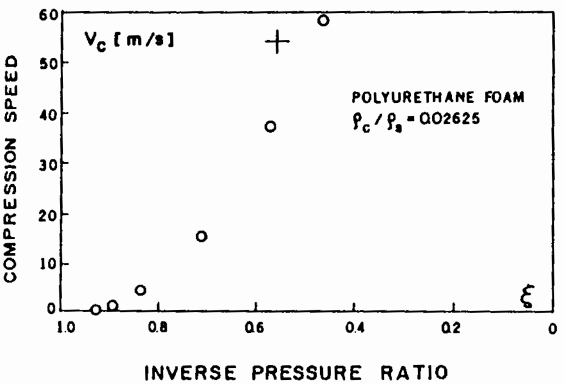

Fig. 10. The dependence of the velocity of the front face of the foam on the inverse shock wave pressure ratio

It should be noted here that the above mentioned experimental fact that the stress-strain relation of the foam depends both on its length and the compression speed could be attributed to the wall friction acting on the foam. Since the material testing machine cannot separate between the stress developed inside the foam and the friction acting along the walls enclosing the foam sample, its reading gives the combined stress of these two phenomena. The fact that the friction forces increase when the foam length increases, due to an increase in the contact area, and decrease when the compression speed decreases, due to a decrease in the friction coefficient, might explain the above experimental observation of an increase in the Young modulus with an increase in the foam length and a decrease in it with an increase in the compression speed. It should further be noted that the fact that the material testing machine gives an effective stress-strain curve of the foam rather than the real one should not be considered as a shortcoming. On the contrary, in order to simulate numerically the phenomenon, the effective rather than the real stress-strain relation should be used. The use of the real stress-strain relation would introduce an inherent error into the simulation results, since, unlike the effective stress-strain relation, it does not include the wall friction which actually affects the phenomenon.

Furthuremore, the strain rate, $\dot{\varepsilon}$, of each measured experimental point, shown in Fig. 8a and 8b, could be calculated by dividing its appropriate compression speed by its appropriate length. If this procedure is applied on the second point in Fig. 8a for which the compression speed is 100 mm/min and the length is 150 mm and to the second point in Fig. 8b for which the compression speed is 50 mm/min and the length is 75 mm one obtains that, inspite the fact that the strain rate is identical for these two experimental data points, their Young modulus is significantly different; while it is about 0.81 MPa for the former it is only 0.31 MPa for the latter. This is in contradiction to reports, for details see Gibson and Ashby (1988), which claim that the stress-strain relation of cellular materials depends on the strain rate.

The speed of sound of a cellular material, a_c, can be calculated from

$$a_c = \sqrt{\frac{E_c}{\rho_c}}, \tag{3}$$

where ρ_c the density of the cellular material can be obtained from

$$\rho_c = (1 - \phi)\rho_s + \phi\rho_p \tag{4}$$

here ρ_s is the density of the material from which the cellular material is made, ρ_p is the density of the fluid filling the pores of the cellular material, and ϕ is the relative volume of the pores in the cellular material, which is also known as porosity, i.e.,

$$\phi = \frac{V_p}{V_c} \tag{5}$$

where V_c is the overall volume of the cellular material, i.e.,

$$V_c = V_s + V_p \tag{6}$$

where V_s and V_p are the volume of the solid the cellular material and the volume of the pores of the cellular material, respectively. Note that it is assumed in (4) to (6) that the cellular material is saturated with only one fluid, i.e., all the pores are completely filled up with a single fluid phase. If the fluid filling the pores is a gas, then $\rho_s \gg \rho_p$ and (4) is simplified to,

$$\rho_c = (1 - \phi)\rho_s \tag{7}$$

from which the porosity could be defined as,

$$\phi = 1 - \frac{\rho_c}{\rho_s} \tag{8}$$

The above mentioned role played significant by the relative density in determining the various properties of a cellular material is again indicated in (8).

The time dependence of the displacement of the front face of the foam as obtained by streak photography, for four different incident shock Mach numbers, is shown in Fig. 9. The steak photographs were taken by an image converter camera (Hadland Photonics IMACON 790) with an argon-ion laser (Spectra-Physics 2030) as light source. The almost perfectly straight trajectories of the front face of the foam indicate that its velocity is almost constant, in agreement

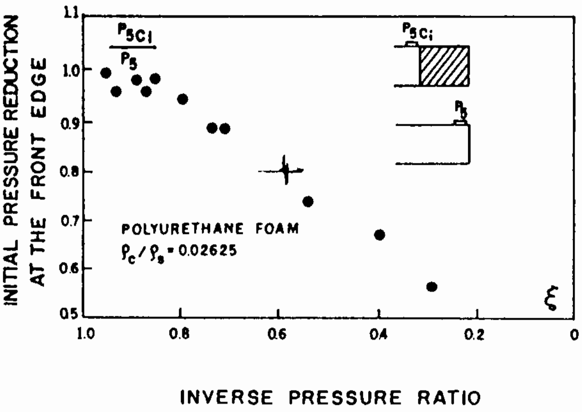

Fig. 11. The dependence of the relative reduction of the initial pressure at the front face of the foam on the inverse shock wave pressure ratio

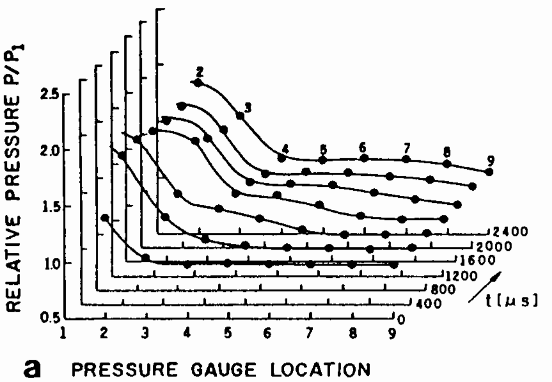

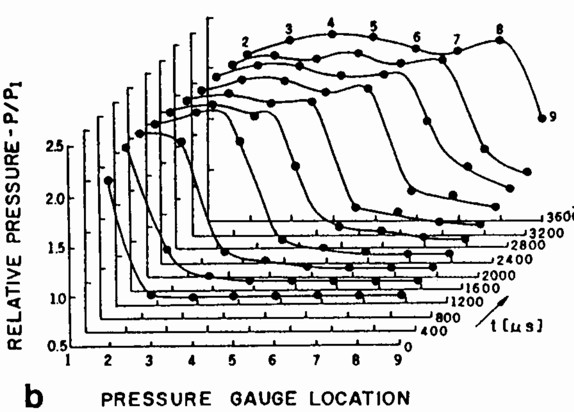

Fig. 12a,b. The pressure distribution inside the foam at different times for: **a** $M_s = 1.04$; **b** $M_s = 1.28$

with the results of Gvozdeva et al. (1985) shown earlier in Fig. 5.

The dependence of compression speed, as deduced from Fig. 9, on the inverse pressure ratio across the incident shock wave, ξ, is shown in Fig. 10. Not suprisingly the compression speed increases as the incident shock Mach number increases.

Inspite the fact that the pressure induced by the reflected shock wave on the front face of the foam, P_{5c}, increases as the incident shock Mach number increases, its value is smaller than the pressure that would have been obtained had the incident shock wave reflected head-on from a solid surface, P_5. The ratio between these two pressures, i.e., P_{5c}/P_5, as a function of the inverse pressure ratio across the incident shock wave is shown in Fig. 11. It is clearly evident from Fig. 11 that the higher the incident shock Mach number, the greater is the attenuation of the initial head-on reflected pressure. However, as will be shown subsequently, when the waves transmitted into the foam collide head-on with the shock-tube end-wall they reflect backwards and eventually emerge from the front face of the foam increasing the gas pressure acting on the front face of the foam to values higher than the values that would have been obtained had the incident shock waves reflected head-on from a solid surface, P_5.

The pressure distibutions, at different time instants, as recorded by the nine pressure transducers, shown in Fig. 6a, are given in Fig. 12a and 12b for $M_s = 1.04$ and $M_s = 1.28$, respectively. The time difference between the pressure distributions is $400\,\mu s$ and the time is measured from the moment when the incident shock waves reached the first pressure transducer. The filled circles in Fig. 12a and 12b indicate the pressure measured by the pressure transducers and the solid line connecting the filled circles is a hand drawn curve fit. The last filled circle in each curve represents the pressurerecorded by pressure transducer No. 9, in Fig. 6a, and the preceeding filled circles corespond to the recordings of pressure transducers Nos. 8, 7, 6, etc. as marked in the pressure distribution appropriate to $t = 4$ ms. It should be noted here that the recorded pressures shown in Fig. 12 (filled circles) do not represent necessarily pressure measurements along the foam. This is due to the fact that as the front face of the foam moves to the right, as a result of the reflected-shock-wave induced pressure, it passes by the pressure transducers, which, as a result, find themselves measuring the pressure in the gaseous phase. Since the pressure across the front face of the foam is continuous the passage of the front face of the foam by the pressure transducer is not visible in the pressure histories recorded by the pressure transducers. For example, extrapolation of the curve appropriate to $M_s = 1.28$ in Fig. 9 indicates that, at $t = 4$ ms, the front face of the foam has been displaced by about 150 mm, as a result, at this time instant, pressure transducers Nos. 1 to 4 are located in the gaseous phase domain and only pressure transducers Nos. 5 to 9 are still located inside the foam. An inspection of the pressure values just ahead of the front face of the foam at different times indicates that, as mentioned earlier, the pressure there in nearly constant. A comparison of the pressure disributions in the two figures indicates that while gradual pressure increases are seen at the lower incident shock Mach number case, i.e., Fig. 12a, much steeper pressure rises are evident for the higher incident shock Mach number case, i.e., Fig. 12b.

As mentioned in Part I of this study when the incident shock wave collides head-on with the front face of the foam it transmits compression waves into the foam. Depending on some condition in Mazor et al. (1992), the compression waves could transform into a shock wave. The results shown in Figs. 12a and 12b suggested that in the moderate incident shock Mach number case, i.e., $M_s = 1.28$, the compression waves almost changed into a shock wave, while at the

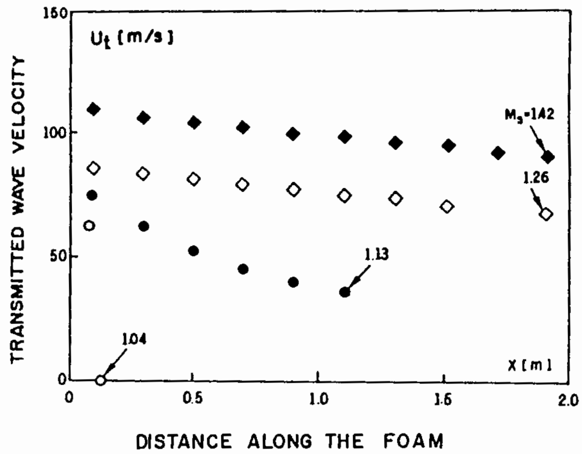

Fig. 13. The dependence of the wave velocity on its propagation distance inside the foam for different incident shock Mach numbers

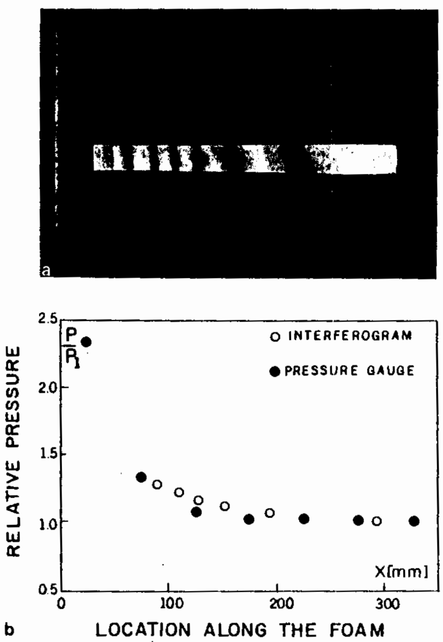

Fig. 14a,b. a A holographic interferogram of the wave propagating inside the foam and **b** comparison of the pressure distribution inside the foam as obtained from pressure and optical measurements

lower incident shock Mach number case, i.e., $M_s = 1.04$ the compression waves did not transform to a shock wave. Note that although this statement seems to be wrong in view of the fact that the convergence conditions given by Mazor et al. (1992) depend solely on the stress-strain relation of thefoam which is, at first sight, identical for the two cases shown in Fig. 12, this is not the case. As shown earlier, in Fig. 8a, the stress-strain relation of the investigated foam was found, in the present experiments, to depend also on the compression speed, which, as shown in Fig. 10, depends on the incident shock Mach number. Consequently, the above reported result regarding the fact that the compression waves did not transform to a shock wave at some incident shock Mach numbers while they almost changed to a shock wave at other incident shock Mach numbers, inspite the fact that the foam, inside which they propagate, was identical, should not be surprising. As a final remark regarding Fig. 12b we would like to note that the pressure profiles do not indicate clearly enough that a shock wave has indeed been formed inside the foam. It merely shows that the pressure gradients has significantly been increased as compared with Fig. 12a. It is possible that the steeper pressure gradient which is evident in Fig. 12a could simply be the result of the higher pressuredifferences which are associated with the higher incident shock Mach numbers.

The recorded wave velocity along a 2 m long foam, as obtained by time counters for four different incident shock Mach numbers, is shown in Fig. 13. It is evident from Fig. 13 that as the transmitted wave propagates inside the foam it attenuates. The smaller the incident shock Mach number, the greater is the attenuation. However, in the case of relatively short foams (less than 0.25 m) and moderate incident shock Mach numbers (greater than about 1.2) it could be quite safely assumed that the transmitted wave velocity remains nearly constant as it propagates along the foam. A probable explanation to this attenuation behavior is given in the Appendix A. It should also be mentioned here that the minimum velocity reported by Henderson et al. (1990) was not evident in the present experiments.

Holographic interferometry was applied in order to understand better the nature of the waves propagating inside the foam. This was achieved by cutting a 20 mm × 250 mm slit along the centerline of the foam as shown in Fig. 6b. A typical holographic interferogram of the transmitted waves inside the foam for the case of $M_s = 1.28$ is shown in Fig. 14a. The fact that the interferogram does not show an evidence of a shock wave should not be surprising since as shown in Fig. 13 the wave velocity in this case is about 80 m/s which is far less than the local speed of sound of the air filling the slit which is about 347 m/s. It should be mentioned here that the influence of the interfaces of the slit on the wave which is transmitted into it has not been investigated and/or evaluated yet. However, based on the results shown in Fig. 14b the influence seems to be in significant.

The relative density difference, $\Delta\rho/\rho_0$, between neighboring fringes is 0.038. If one assumes that the entropy along the streamlines is constant then the relative pressure difference, $\Delta P/P_0$ between the neighboring fringes is 0.0536. The pressure distribution as obtained from the holographic interferogram, using this assumption, together with the pressure distribution as obtained from the measurements of the Kistler pressure transducers is shown in Fig. 14b. The good agreement between the two pressure distributions clearly indicates that flow visualization techniques together with the experimental set-up shown in Fig. 6b could be successfully used to investigate the nature of the pressue waves which are developed and propagate inside the foam.

2.2. *The numerical study*

The basic details of the numerical method and approach which were adopted throughout the course of this study were

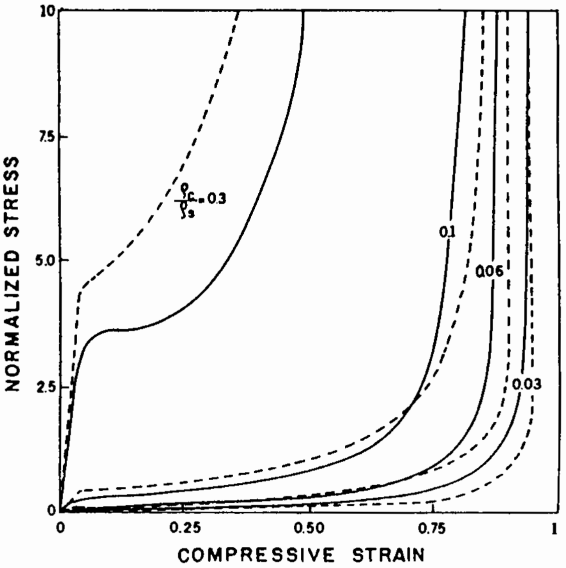

Fig. 15. Stress-strain map of foams as obtained from our empirical model. Solid lines – Gibson and Ashby's (1988) experimental results, dashed line – predictions of Mazor et al.'s (1993) empirical model.

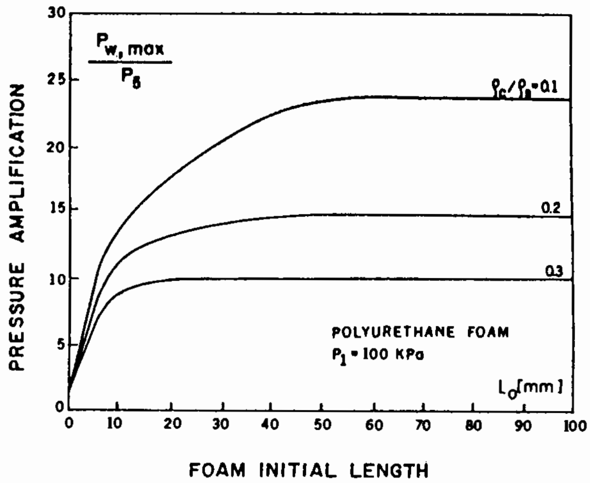

Fig. 16. The dependence of the peak pressure at the shock-tube end-wall on the initial lengh of the foam and its relative density (numerical results)

outlined in Mazor et al. (1992). As shown there, the set of the governing equations of the considered problem consists of ten equations of which only one, namely the constitutive relation of the cellular material, i.e., $\sigma = \sigma(\varepsilon)$, depends on the specifics of the cellular material. Consequently, since the considered cellular material is an open cell polyurethane foam there is a need to use its appropriate, stress-strain relation.

Gibson and Ashby (1988) who described in detail the stress-strain relations of foams, in general, and those of open and closed cell polyurethane foams, in particular, presented, in chapter 5 of their book, an experimentally measured map of stress-strain curves, in which the relative density of the foam was a parameter, for the case of a uni-axial stress compression. In addition, they proposed a set of empirical relations, based on solid mechanics considerations, by which they claimed to produce a similar "theoretical" map of stress-strain curves. Unfortunately, all our attempts to reproduce their "theoretical" map, using their empirical relations, failed. The failure was due to the fact that their empirical relations were not "tailored" appropriately at their edges. As a result, based on their solid mechanics considerations and general formulation, a well-tailored set of empirical equations was developed by us. For the reader's convinience it is listed in the following:
in the linear elastic domain, i.e., $0 \le \varepsilon \le 0.05$,

$$\sigma = E_c\varepsilon; \tag{9}$$

in the elastic-plastic (plateau) domain, i.e., $0.05 \le \varepsilon \le \varepsilon_d$,

$$\sigma = 0.05E\frac{\varepsilon_d}{\varepsilon_d - \varepsilon + 0.05}; \tag{10}$$

in the densification domain, i.e., $\varepsilon_d \le \varepsilon < 1$,

$$\sigma = E_c\varepsilon_d + E_s\frac{\varepsilon - \varepsilon_d}{1 - \varepsilon_d}, \tag{11}$$

where

$$E_c = E_s\left(\frac{\rho_c}{\rho_s}\right)^2 \tag{12}$$

and

$$\varepsilon_d = 1 - 1.4\frac{\rho_c}{\rho_s}. \tag{13}$$

More details regarding these relations can be found in Mazor et al. (1993). A revised map of stress-strain curves as obtained using the above suggested relations together with the experimental curves of Gibson and Ashby (1988) is shown in Fig. 15. Not only that the above ralations, unlike those given by Gibson and Ashby (1988), are well-tailored and enables one to obtain the stress-strain curves, a comparison of Gibson and Ashby's "theoretical" with our empirical map indicates that our suggested stress-strain relations result in a better agreement with the experimental results at large strains, e.g., compare the curves for $\rho_c/\rho_s = 0.1$.

Similarly, a set of well-tailored empirical stress-strain relations, for the case of a uni-axial strain compression mode, were also developed. They are: in the linear elastic domain, i.e., $0 \le \varepsilon \le \varepsilon_1$,

$$\sigma = E_c\varepsilon; \tag{14}$$

in the elastic-plastic (plateau) domain, i.e., $\varepsilon_1 \le \varepsilon \le \varepsilon_d$,

$$\sigma = 0.041E_s\left(\frac{\rho_c}{\rho_s}\right)^2\frac{\varepsilon_d}{\varepsilon_d - \varepsilon + \varepsilon_1}; \tag{15}$$

in the densification domain, i.e., $\varepsilon_d \le \varepsilon < 1$,

$$\begin{aligned}\sigma &= 0.041E_s\left(\frac{\rho_c}{\rho_s}\right)^2\frac{\varepsilon_d}{\varepsilon_1}\\ &\quad + E_s\left(1 - \frac{2\nu_s^2}{1 - 2\nu_s}\right)^{-1}\frac{\varepsilon - \varepsilon_d}{1 - \varepsilon_d},\end{aligned} \tag{16}$$

where

$$E_c = E_s \left(\frac{\rho_c}{\rho_s}\right)^2 \frac{1}{1+\dfrac{\rho_c}{\rho_s}} \left(1 - \frac{2\nu_c^2}{1-2\nu_c}\right)^{-1}, \tag{17}$$

and

$$\varepsilon_1 = 0.041 \left(1 - \frac{2\nu_c^2}{1-\nu_c}\right) \left(1 + \frac{\rho_c}{\rho_s}\right), \tag{18}$$

and in similar to (13)

$$\varepsilon_d = 1 - 1.4\frac{\rho_c}{\rho_s}. \tag{19}$$

The only parameter in the above set of equations which has not been defined yet is ν_s which is the Poisson ratio of the solid material from which the cellular material is made. In addition, based on Gibson and Ashby (1988) the most appropriate Poisson ratio for a polyurethane foam, i.e., ν_c, is 1/3.

As mensioned in Mazor et al. (1992) when the incident shock wave collides head-on with the front face of the cellular material it transmits into the foam compression waves which can transform to a shock wave provided the stress-strain relation of the cellular material fulfills the following two conditions,

$$\frac{\partial \sigma}{\partial \lambda} > 0, \tag{20}$$

and

$$\frac{\partial^2 \sigma}{\partial \lambda^2} > 0. \tag{21}$$

Applying the above transformation conditions on the stress-strain relation in the linear-elastic domain, as given by (14), indicates that while the condition given by (20) is satisfied, the one given by (21) is not. Consequently, as long as the investigated foam is in its linear elastic domain the compression waves cannot transform to a shock wave. This is in agreement with Henderson et al. (1990) who showed that the wave transmitted initially into their investigated foam was not a shock wave but a band of compression waves. The velocity, V_c, of the compression waves, in the linear elastic domain, can be obtained by inserting (15) into (3),

$$V_c = a_c = \sqrt{\frac{E_s}{\rho_s}\frac{\rho_c}{\rho_s}\frac{1}{1+\dfrac{\rho_c}{\rho_s}}\left(1 - \frac{2\nu_c^2}{1-\nu_c}\right)} \tag{22}$$

Equation (22) indicates that for a given foam material the velocity of the transmitted compression waves depends on the relative density of the foam.

Applying the convergence conditions on the stress-strain relation in the elastic-plastic domain, as given by (15), indicates that both of them are satisfied. Therefore, if the foam reaches this domain the compression wave transmitted into it can transform to a shock wave depending on whether the foam is long enough to enable them to transform. It should be noted here that this result indicates a unique feature of foams, since they are the only known materials

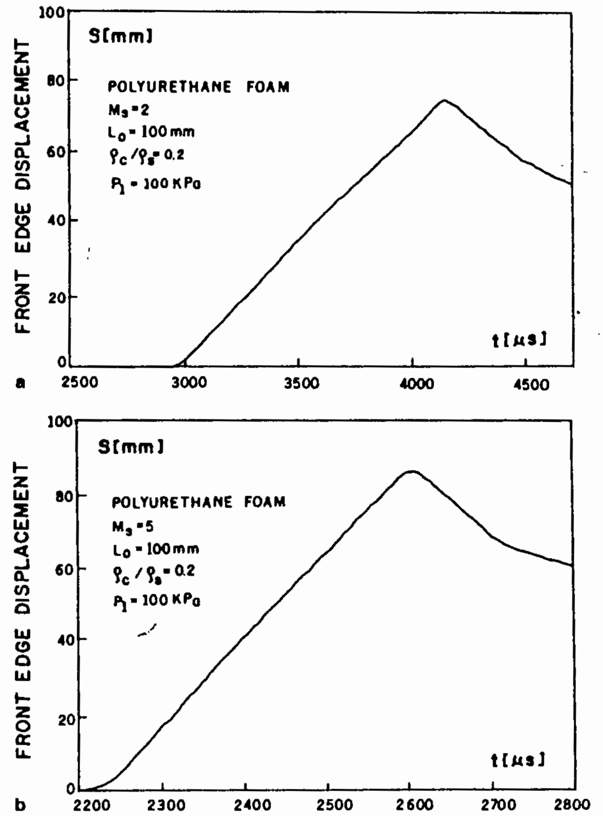

Fig. 17a,b. The displacement of the front face of the foam, as predicted by the numerical simulation, for **a** $M_s = 2$ and **b** $M_s = 5$

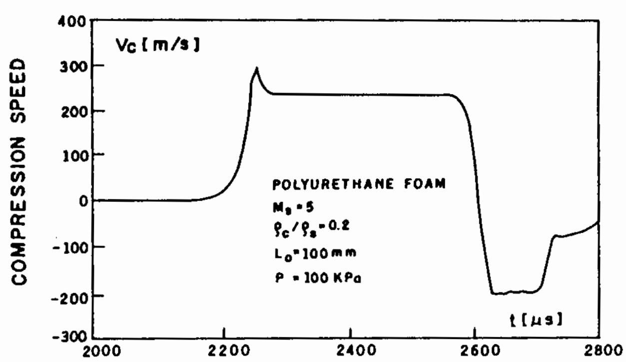

Fig. 18. The velocity of the front face of the foam, as predicted by the numerical simulation for $M_s = 5$

in which a shock wave can be generated during a uni-axial strain compression.

Applying the above convergence conditions on the stress-strain relation in the densification domain, as given by (16), indicates that while the condition given by (20) is satisfied, the one given by (21) isnot. Consequently, Compression waves propagating in a foam which is in its densification domain cannot transform to a shock wave. The velocity, V_c, of the compression waves, in the densification domain, can be simply obtained by inserting (16) into (3),

$$V_c = a_c = \sqrt{\frac{E_s}{\rho_c}\left(1 - \frac{2\nu_s^2}{1-\nu_s}\right)}$$

Since the densification domain is reached after all the pores have completely colapsed it is not suprising that the relative density does not play any role in determining the wave velocity at this stage of the compression which follows the elastic-plastic domain.

During the course of the present numerical study the governing equations were solved for a flexible open cell polyurethane foam having the following relative densities; $\rho_c/\rho_s = 0.1$, 0.2, and 0.3. In addition, in order to verify and better understand the experimental results of Gvozdeva et al. (1985), shown in Fig. 3, four different initial lengths were assigned to the foam, i.e., $L = 10$, 20, 50, and 100 mm. The head-on interaction was simulated for the above parameters and two incident shock Mach numbers, i.e., $M_s = 2$ and 5. The initial conditions ahead of the incident shock wave were, $u_{g_1} = 0$, $P_1 = 100\,\mathrm{kPa}$ and $T_1 = 300\,\mathrm{K}$. The cross section of the foam was set to be $0.01\,\mathrm{m}^2$ and the properties of the flexible polyurethane foam as taken from Gibson and Ashby (1988) were $\rho_s = 1100\,\mathrm{kg/m}^3$, $E_s = 45\,\mathrm{MPa}$, and $\nu_s = 0.45$.

The peak pressure developed at the shock-tube end-wall, $P_{w,max}$, behind the foam, relative to the pressure which would have been developed there, had the incident shock wave reflected directly from the shock-tube end-wall, P_5, as afunction of the initial length of the foam, L_0, for different relative densities, ρ_c/ρ_s, is shown in Fig. 16 for the case of an incident shock wave having a Mach number, $M_s = 2$, which collides head-on with a polyurethane foam. In general, the results resemble those obtained by Gvozdeva et al. (1985) which are reproduced in Fig. 3, i.e., an increase in $P_{w,max}$ as L_0 increases until a certain critical value of L_0 after which $P_{w,max}$ reaches an asymptotic value. Note that Fig. 16 indicates that this critical length increases as the relative density of the foam decreases. In addition, it is also evident in Fig. 16, that the smaller the value of the relative density, the larger is the obtained peak pressure at the end-wall, e.g., by decreasing the relative density first from 0.3 to 0.2 and then to 0.1 the relative peak pressure increases first from about 10 to about 15 and then to about 23.5. This could be attributed to the fact that foams having smaller relative densities are easier to accelerate and hence they reach higher material velocities which evetually translate into higher "stagnation" pressures at the end-wall. It should be noted here that this fact is incorrect when the relative density tends to zero. The lowest value of the relative density for which the presented physical model is applicable is yet to be determined. This can be done by comparing the predictions of the present simulation with actual experimental results.

The displacement of the front face of a foam having an initial length $L_0 = 100\,\mathrm{mm}$ and a relative density $\rho_c/\rho_s = 0.2$ after being collided head-on with incident shock waves having Mach numbers $M_s = 2$ and $M_s=5$ are shown in Fig. 17a and 17b, respectively. Similar to the results of Gvozdeva et al. (1985), which have been reproduced in Fig. 5, and to the present experimental results, shown in Fig. 9, here too the trajectories of the front faces of the foams are almost straight lines. The average velocities of the front faces of the foams, as measured from Fig. 17a and 17b are about 64 m/s and 220 m/s, respectively. The front face velocity as measured from Gvozdeva et al.'s (1985) result, for $M_s = 2$, is about 128 m/s. The fact that the velocity measured in Gvozdeva et al.'s (1985) experiment is twice as large as that predicted by the numerical code, inspite the fact that the incident shock Mach numbers are the same, could be attributed to the earlier mentioned fact that the relative density of the foam in Fig. 5 is somewhere in the range $0.02 \div 0.05$ while that of the foam in Fig. 17a is 0.2. The $4 \div 10$ times smaller relative density could be rersponssible for the 100 % increase in the front face velocity. The 3.5 times increase in the front face velocity of the same foam when the incident shock Mach number is changed from 2 to 5 is self explanatory if one recalls the that pressure ratio behind the head-on reflecting shock wave, P_{5c}/P_1, increases from about 13 to about 150 (see Fig. 19 and subsequent discussion). It is also interesting to note that the front face trajectory deviates from an almost straight line behavior only at the initial stage of the motion when, the front face accelerates to reach its almost constant velocity. As mentioned earlier, at this stage the foam is still in its linear-elastic domain inside which its stress increases when its strain increases.

The velocity of the front face of a foam having an initial length $L_0 = 100\,\mathrm{mm}$ and a relative density $\rho_c/\rho_s = 0.2$ after being collided head-on with an incident shock wave having a Mach number $M_s = 5$ (i.e., the same as that shown in Fig. 17b) is shown in Fig. 18. The above mentioned strong acceleration atthe early stages of the compression, followed by a weak deceleration to reach analmost constant velocity of about 220 m/s for about 350 μs is clearly evident. It is also seen in Fig. 18 that the almost constant velocity motion is terminated by a strong (almost constant) decelaration which eventually causesthe front face of the foam to reverse its direction of motion and to atain an almost constant velocity of about 200 m/s in the opposite direction.

The pressure histories on the front face of the foam having an initial length $L_0 = 100\,\mathrm{mm}$ and a relative density $\rho_c/\rho_s = 0.2$, after being collided head-on with incident shock waves having Mach numbers $M_s = 2$ and $M_s = 5$ are shown in Fig. 19a and 19b together with the pressures which would have been obtained had the incident shock waves reflected head-on from a solid wall. The initial pressures induced by the shock waves reflecting head-on from the front faces of the foams are seen to reach only 86 % and 79 % of the values appropriate to the the head-on reflections of the same incident shock waves, $M_s = 2$ and $M_s = 5$, respectively, from a solid wall. It is also seen in Fig. 19a and 19b that the above mentioned pressure increases at the front faces are followed by secondary pressure increases which are caused by the shock waves which emerge out of the foams. These shock waves are the results of the head-on reflections of the transmitted shock waves at the shock-tube end-wall. When the reflected shock waves reach the front faces of the foam they reflect backwards into the foam as rarefaction waves and transmit shock waves into the gaseous phase. The transmitted shock waves result in the second pressure increases at the front faces of the foam (as shown in Fig. 19a and 19b) and the reflected rarefaction waves terminate the compression phase of the foam by reversing its direction of motion (as shown in Fig. 18). The emergence of the shock waves from the front faces of the foam is about

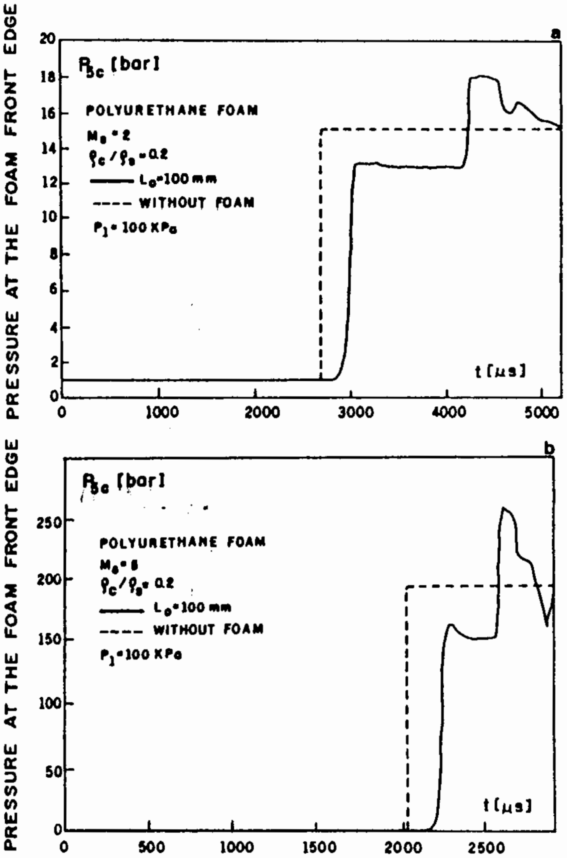

Fig. 19a,b. The pressure history at the front face of the foam, as predicted by the numerical simulation, for **a** $M_s = 2$ and **b** $M_s = 5$

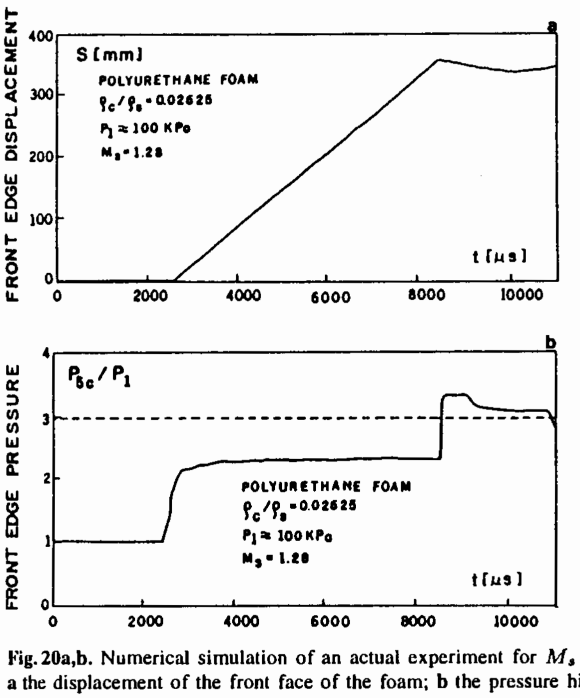

Fig. 20a,b. Numerical simulation of an actual experiment for $M_s = 1.28$: **a** the displacement of the front face of the foam; **b** the pressure history at the front face of the foam

1125 and 350 μs after the interactions started, in accordance with the durations of the constant velocity phases shown in Fig. 17a and 17b, respectively (the straight portions of the displacement curves). It is also evident from Fig. 19a and 19b that as a result of the emergence of these shock waves the pressures at the front faces of the foam reach values which are about 20% and 35% higher than those appropriate to the head-on reflection from a solid wall.

Based on manufacturer's data i.e., $\rho_c/\rho_s = 0.02625$, see the experimental section of this study, and Fig. 7 from which a typical Young modulus of the foam can be measured, in its linear elastic regime, to be E_c = 0.134 MPa and with the aid of (17) the Young modulus of the polyurethane from which the foam was made was determined to be about E_s = 194.5 MPa. Using these values in our numerical code together with the following initialal data;
incident shock Mach number $M_s = 1.28$;
initial pressure P_1 = 100 kPa;
initial temperature T_1 = 300 K;
initial foam length of L_0 = 400 mm; and
a foam cross section of 9000 mm^2,
resulted in, the front face displacement, shown in Fig. 20a, and the pressure history at the front face of the foam, shown in Fig. 20b. It could be deduced from Fig. 20a that the compression speed of the foam is about 55 m/s and that the pressure actin g on its front face, P_{5c}, is about $0.77P_5$. This values which have been added (as a cross signs) to Figs. 10 and 11, respectively, resemble a poor agreement with the measured compression speeds and a very good agreement with the measured pressures. The poor agreement with the compression speed could be attributed to the unknown correct value of the Young modulus of the foam. As mentioned earlier (see Fig. 8a and the appropriate discussion) the Young modulus of the foam was found, in the present experiments, to depend on the compression speed. The value used in the present computation was deduced from Fig. 7 in which the compression speed is 0.833×10^{-3} m/s while the actual compressionn speed is in the order of 50 ÷ 150 m/s. This difference of about five orders of magnitude could explain the over-predicted value of the compression speed. Note that as mentioned earlier the value of the Young Modulus as deduced by us was E_s = 194.5 MPa, however, as quoted by Gibson and Ashby (1988) the Young modulus of polyurethane PU(R) foams is about six time larger, i.e., 1200 MPa. Replacing only this value in the numerical computation results in a compression speed of about 48 m/s (as compared to about 55 m/s in the previous computatoion and to about 38 m/s in the experiment) and a presssure of about $0.79P_5$ (as compared to about $0.77P_5$ both in the previous computation and the experiment). Hence, it is quite clear from these computations that while the Young modulus has a noticable influence on the compression speed it has a negligible effect on the pressure acting on the front face of the foam.

It should also be mentioned here that when the measured stress-strain curve (see Fig. 7) is drawn on Gibson and Ashby's (1988) experimental stress-strain map, in which the relative density of the foam is a parameter, the presently measured stress-strain curve agrees best with the curve for which the relative density, ρ_c/ρ_s, is about 0.06. In addition to the fact that this value is more than twice larger than the value quoted by the manufacturer, i.e., 0.02625, one should recall that the relative density is the most important property of a foam. Consequently, having its correct value is most essencial if one wishes to acurately simulate the interaction.

It should also be mentioned that based on Fig. 20b about 6000 μs after the interaction started the above mentioned secondary shock wave emerges out of the foam resulting in an increase in the pressure to a value larger by about 12 % than the value which would have been obtained had the incident shock wave reflected head-on from a solid wall.

3. Summary and conclusions

The head-on interaction of a planar shock wave with an open cell foam has been investigated both experimentally and numerically for the case of a uni-axial strain compression. The numerical predictions were found to qualitatively agree both with our and others experimental results. A quantitative comparison could not be made since the computer code requires the knowledge of some properties ofthe foam which unfortunately could not be measured. Consequently, in order to overcome this shortcoming there is a need to develop some experimental techniques which will enable one to obtain the mechanical properties of the foam which are required by the computer code.

The major conclusions regarding the investigated interaction are,

(1) The stress-strain relation of a foam depends on:
   i) its mechanical behavior in the plateau domain (elastomeric, elastic-plastic or elastic-brittle);
   ii) its internal structure (open or closed cell);
   iii) its compression mode (uni-axial stress, bi-axial stress or uni-axial strain);
   iv) its compression speed; and
   v) its initial lengh.

(2) Different stress-strain relations were obtained for identical strain rates.

(3) Due to the presence of the foam the induced pressure on the shock-tube end-wall is enhanced as compared to the pressure which is obtained without a foam:
   i) the pressure enhancement increases as the relative density of the foam decreases;
   ii) the pressure enhancement increases as the initial length of the foam increases until a critical length beyond which the pressure enhancement remains unchanged; and
   iii) the critical length increases as the relative density decreases.

(4) During the compression phase, the front face of the foam moves with an almost constant velocity:
   i) the velocity is larger when the relative density is smaller;
   ii) the velocity is larger when the incident shock Mach number is larger; and
   iii) the time duration of the almost constant velocity is shorter when the incident shock Mach number is larger.

(5) During the relaxation (decompression) phase, the front face of the foam moves with an almost constant velocity in a direction opposite to that during the compression phase.

(6)
   i) At the early stages of the interaction, the pressure induced on the front face of the foam, P_{5ci}, is smaller than the pressure induced by a shock wave reflecting head-on from a solid wall, P_5;
   ii) as the incident shock Mach number increases P_{5ci}/P_5 decreases;
   iii) at a later stage of the interaction, the pressure induced on the front face of the foam, P_{5cf}, increases beyond the pressure induced by a shock wave reflecting head-on from a solid wall, P_5; and
   iv) as the incident shock Mach number increases P_{5cf}/P_5 increases.

(7) The propagation velocity of the wave inside the foam decreases as the wave progresses.

(8) Based on the stress-strain relation of foams:
   i) the transmitted compression waves cannot transform to a shock wave while the foam is in its linear elastic domain;
   ii) the transmitted compression waves cannot transform to a shock wave while the foam is in its densification domain;
   iii) the transmitted compression waves can transform to a shock wave while the foamis in its plateau domain; and
   iv) foams are the only known materials in which the compression waves can transform to a shock wave in a uni-axial strain compression.

(9) As shown in the Appendix, the attenuation of the transmitted wave as it travells inside the foam can be related to the wave impedances.

Finally, it is the authors' belief that there is still a need to further investigate this phenomenon, both experimentally and numerically, in order to better understand it.

Appendix A: The role of the wave impedance in determining the attenuation of the transmitted wave inside the foam

It was shown in Fig. 13 that while the transmitted waves which result from the head-on collision of weak incident shock waves decay very quickly as they propagate along the foam those which result from the head-on collision of moderate incident shock wave do not experience such a strong attenuation.

Let us first define a parameter E_{ti} which is a measure of the ratio of the energy change across the incident shock wave and that across the transmitted wave, i.e.,

$$E_{ti} = \frac{\Delta P_t \Delta u_t}{\Delta P_i \Delta u_i} = \frac{(P_t - P_1)(u_t - u_1)}{(P_2 - P_1)(u_2 - u_1)} \tag{A.1}$$

where as indicated in Fig. A.1, P_1 is the pressure ahead of the incident shock wave, in the gaseous phase, and that ahead of the transmitted wave, insidethe foam, P_2, P_t are the pressures behind these incident and transmitted waves, respectively, u_1 is the velocity of the gas ahead of the incident shock wave and the velocity of the foam ahead of the transmitted wave (it is actually equal to zero in the present study), u_2 and u_t are the velocities of the gas behind

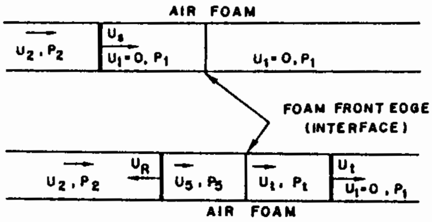

Fig. A.1. Definition of flow regions and flow parameters

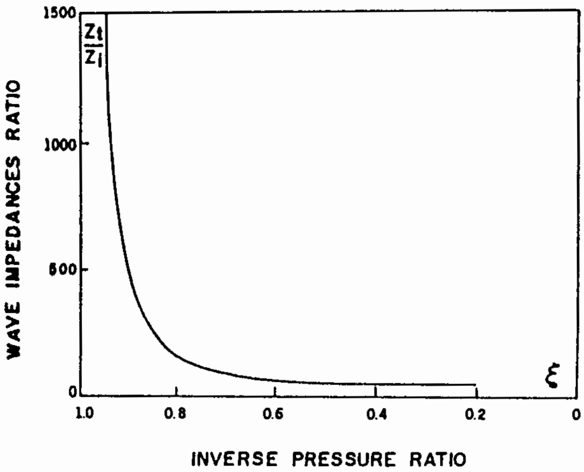

Fig. A.2. Dependence of the wave impedances ratio on the inverse pressure ratio across the incident shock wave

the incident shock wave and the foam behind the transmitted wave, respectively. Equation (A.1) could be rewritten as

$$E_{ti} = \frac{(P_t - P_1)^2 Z_i}{(P_2 - P_1)^2 Z_t} \tag{A.2}$$

where Z_i and Z_t are the wave impedances of the incident shock wave and the transmitted wave, respectively, i.e.,

$$Z_i = \frac{\Delta P_i}{\Delta u_i} = \frac{P_2 - P_1}{u_2 - u_1} \tag{A.3}$$

$$Z_t = \frac{\Delta P_t}{\Delta u_t} = \frac{P_t - P_1}{u_t - u_1} \tag{A.4}$$

Assuming that the pressures and the velocities on both sides of the front face of the foam are equal one can rewrite (A.4) as

$$Z_t = \frac{\Delta P_t}{\Delta u_t} = \frac{P_5 - P_1}{u_5 - u_1} \tag{A.5}$$

where P_5 and u_5 are the gas pressure and velocity behind the head-on reflecting shock wave (see Fig. A.1). The dependence of the ratio between the wave impedances, as calculated from (A.3) and (A.4), on the inverse pressure ratio across the incident shock wave, ξ, is shown in Fig. A.2. Itis evident from Fig. A.2 that as ξ exceeds 0.8 and approaches unity the ratio Z_t/Z_i approaches infinity and E_{ti} approaches zero. In other words, when the incident shock wave is weak the transmitted wave decay quickly as the energy change across it vanishes. The opposite is the case for moderate incident shock waves ($\xi < 0.7$, i.e., $M_s > 1.17$ as seen in Fig. A.2). In this case the ratio Z_t/Z_i reaches a finite value which in turn results in a situation in which the energy change across the transmitted wave has a finite non-zero value which in turn results in an almost non-attenuating wave.

References

Baer MR (1992) A numerical study of shock wave reflections on low density foam. Shock Waves 2:121–124

Gibson BE, Ashby MF (1988) Cellular solids: stucture and properties, 1st edn. Pergamon Press

Gvozdeva LG, Faresov YuM, Fokeev VP (1985) Interaction between air shock waves and porous compressible materials. Sov Phys Appl Math and Tech Phys 3:111–115

Henderson LF, Virgona RJ, Di J, Gvozdeva LG (1990) Refraction of a normal shock wave from nitrogen into polyurethane foam. In: Kim YW (ed) Current topics in shock waves. American Institute of Physics, New York, pp 814–818

Mazor G, Ben-Dor G, Cederbaum G, Igra O (1993) Well tailored compressive stress-strain relations for elastomeric foams, submitted for publication

Mazor G, Ben-Dor G, Igra O, Sorek S, Takayama K (1992) Shock wave interaction with cellular materials. Part: I analytical investigation and governing equations. Shock Waves, submitted for publication

Mazor G, Igra O, Ben-dor G, Mond M, Reichenbach H (1992) Head-on collision of normal shock waves with a rubber supported wall. Proc Roy Soc Lond, Ser A, to be published

Skews BW (1991) The reflected pressure field in the interaction of weak shock waves with a compressible foam. Shock Waves 3:205–211

Skews BW, Atkins MD, Seitz MW (1992) Gas dynamic and physical behaviorof compressible porous foams struck by weak shock waves. In: Takayama K (ed) Shock waves – Proc 18th Intl Symp on Shock Waves. Springer-Verlag, Heidelberg, pp 511–516

This article was processed using Springer-Verlag TEX Shock Waves macro package 1.0 and the AMS fonts, developed by the American Mathematical Society.